Chiral Vector Determination of Carbon Nanotubes by Observation of Interference Patterns Near the End Cap

Masayuki Furuhashi[1] and Tadahiro Komeda[1,2,*]

[1]*IMRAM, Tohoku University, 2-1-1, Katahira, Aoba, Sendai, 980-0877, Japan*
[2]*JST, CREST, 5,Sanbancho, Chiyoda-ku, Tokyo, 102-0075, Japan*

(Received 12 February 2008; published 31 October 2008)

We have observed clear interference images near the end caps of semiconducting carbon nanotubes with quasiarmchair and zigzag chiral vectors, using a scanning tunneling microscope. We performed a simple tight-binding calculation to simulate the interference patterns, in which Bloch states with $\boldsymbol{k}$ and $-\boldsymbol{k}$ wave vectors were superimposed. The calculations were able to reproduce the observed interference patterns. In addition, we demonstrated that the interference patterns can be categorized by the positions of $\boldsymbol{k}_{\mathrm{min}}$ in the Brillouin zone that yield minimum energy in the conduction band, and can give information on the chiral vector of a carbon nanotube.

DOI: 10.1103/PhysRevLett.101.185503 PACS numbers: 61.46.−w, 07.79.−v, 42.25.Fx

Carbon nanotubes (CNT) are considered to be the most prominent candidate for future electronic materials [1–3], wherein control of molecular-orbital level properties is required. Scanning tunneling microscopy (STM) has played an important role in atomic scale characterization. In particular, observations of the standing wave formed by the interference of an electronic state of CNT have clearly visualized the wave functions of CNTs [4,5], and have revealed electrical properties, such as the band structure [6,7].

In this Letter, we discuss the interference patterns observed in the vicinity of the terminal of CNTs (often referred to as the end cap). The patterns are sensitive to the way of the wrapping, which is characterized by a chiral vector ($\boldsymbol{C}_h$) of the CNTs [3]. First, we experimentally show high-resolution STM images of semiconducting CNTs that have chiralities close to the zigzag and the armchair. We observed a clear interference pattern near the end cap, which is characteristic for each chirality. Second, we describe the simulation of these patterns with a tight-binding approximation and by simply superimposing a Bloch state (translational vector $\boldsymbol{k}_{\mathrm{min}}$) and its scattered wave ($-\boldsymbol{k}_{\mathrm{min}}$) that corresponds to the valence band maximum (the conduction band minimum). The results of the simulation were able to reproduce the observed patterns. Finally, we analyzed the relationship between the positions of $\boldsymbol{k}_{\mathrm{min}}$ in the Brillouin zone and the interference pattern. Since the $\boldsymbol{k}_{\mathrm{min}}$ positions are sensitive to the chiral vectors, the observation of an internal diffraction pattern for the CNTs can play a complementary role in the chiral vector determination to direct observation of the atomic structure of a CNT.

Experimentally, we prepared a sample by depositing purified single wall CNTs (Carbon Nanotechnologies Inc., U.S.) dispersed in 1,2-dichloroethane on an Au (111)/mica surface, which was cleaned by Ar^+ sputtering and annealed prior to the deposition. After being introduced into a UHV chamber, the sample was annealed at 220 °C for 1 h in order to remove any residual solvent. STM observations were carried out using a JSTM-4500XT instrument (JEOL, Japan) cooled with liquid nitrogen under UHV conditions.

We first show STM images of an armchair CNT. In Fig. 1(a), the image is shown in a derivative mode to flatten the background. In the upper panel in Fig. 1(a), the end cap lies on the left-hand side and the infinite tube extends to the right. Two different features can be seen in the left- and right-hand sides, and a transition appears at ~6 nm from the end cap. The lower panel in Fig. 1(a) shows a magnified view of this transition region. The periodic pattern on the right-hand side corresponds to the ''normal'' structure of the CNT, in which hexagonal rings surrounding the dark areas correspond to the hexagonal network of the CNT (superimposed in the lower panel). The observed hexagonal unit is slightly distorted since the tip has scanned a cylindrical tube surface [8,9]. The overall appearance agrees with those reported previously [10,11]. From the periodic pattern, we can estimate a chiral angle of ~2.9° and a tube diameter of ~1.9 nm, from which the most plausible chiral vector of (28, −13) can be deduced. Since this CNT is close to an armchair type, the CNT axis is close to the ΓK direction in $\boldsymbol{k}$ space.

Near the end cap, on the other hand, we observe a characteristic structure with a complex pattern. This structure can be described as a combination of aligned bright spots and wavy lines sandwiched by the former. The alignment is indicated by thin lines in the figure, which are rotated 60° from the tube axis. The wavy patterns are also aligned along the thin lines. The separation of the bright spots (pointed by upper ends of the bars) along the CNT axis is ~0.72 nm, which is close to $3a$ ($a = 0.246$ nm, the lattice constant of graphene). This agrees with the interference periodicity discussed in metallic CNT [4,6,12], wherein the energy band crosses the Fermi level at the K point that corresponds to $\boldsymbol{k} = 2\pi/3a$.

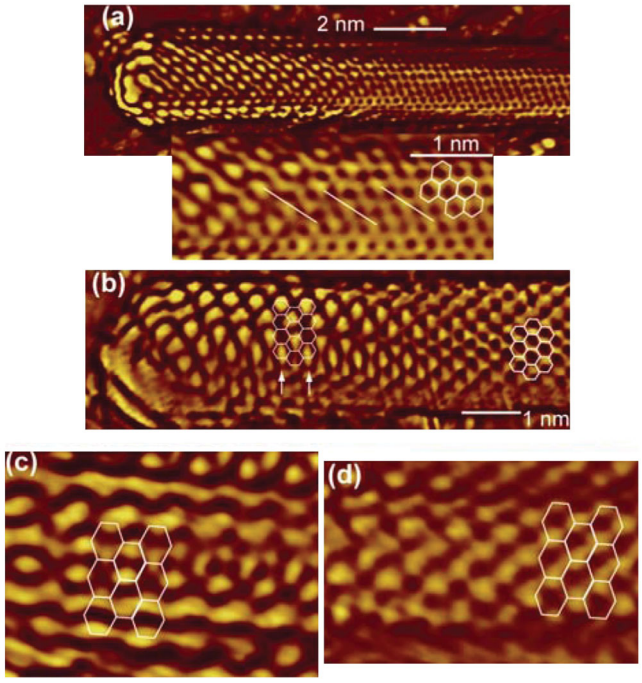

FIG. 1 (color). (a) Upper panel: Interference pattern observed near the end cap of armchairlike semiconducting CNT [chiral vector $(28, -13)$], ($I_t = 100$ pA $V_{\text{bias}} = 0.6$ V). Lower panel: Magnified image of the upper panel. The thin lines are included as a guide to the eye for the aligned bright spots. The superimposed hexagons are the primitive honeycomb structures. (b) Interference patterns for the zigzag CNT ($I_t = 100$ pA $V_{\text{bias}} = 0.7$ V). Bright spots separated by $4\boldsymbol{a}$ along the arrows. (c),(d) Bias dependence of an interference pattern of the zigzag CNT measured with $I_t = 100$ pA and (c) $V_{\text{bias}} = 0.7$ V, (d) $V_{\text{bias}} = 1.0$ V at an identical position of the same CNT [chiral vector $(15, -1)$].

Next, we show STM observations for a CNT whose chirality is close to zigzag. A typical STM image near the end cap is shown in Fig. 1(b). Similar to Fig. 1(a), an intriguing pattern can be observed within ~6 nm from the end cap. In the right-hand side area, we can see a hexagonal network rotated 30° from the armchair. The CNT axis is aligned to the ΓM direction of the Brillouin zone. On the left-hand side, we can notice a pattern of bright spots with a large periodicity perpendicular to the tube axis. Along the thin arrows, we note bright spots with a separation of $\sim 4\boldsymbol{a}$ (see superimposed hexagons). Along a line between the two, two bright spots are separated by $\boldsymbol{a}$.

We show STM images of another zigzag CNT in Fig. 1(c) imaged at $V_{\text{bias}} = 0.7$ V, which exhibits more minute features. The CNT has a chirality close to the zigzag but slightly different from Fig. 1(b), which we assigned as $(15, -1)$. Isolated bright dots are aligned along the thin line A in the figure. Below line A, there is a wavy line in the horizontal direction. We can also observe aligned dots which are above line A by $\boldsymbol{a}$.

When the same CNT was observed with $V_{\text{bias}} = 1.0$ V, the image shows a 1×1 pattern even near the end cap. This is shown in Fig. 1(d), which was obtained in the same area as the CNT in Fig. 1(c). This is caused primarily by a mixture of various electronic states contained in the allowed energy region.

Next, we describe the simulation method employed to account for the interference pattern. For this, we briefly mention the electronic structure of a CNT. Though the electronic structure of a CNT is close to that of graphene, limited $\boldsymbol{k}$ points are allowed due to quantization of an electron in the wrapping direction. The allowed $\boldsymbol{k}$ points can be plotted on straight lines along the tube-axis direction, separated by $2\pi/|\boldsymbol{C}_h|$ from each other. In Fig. 2(a), we show an example of such lines for a CNT with a chirality of $(4, 2)$. These are shown by long black lines. An equivalent expression is a series of short bars whose lengths are an inverse of the translational vector, which are also shown in Fig. 2(a) by the short red lines. It has been demonstrated that if the chiral vector (n, m) satisfies the condition of $n - m = 0 \pmod 3$, the CNT is metallic and the energy band $[E(k)]$ curve crosses the Fermi level at K or K'. For a semiconducting CNT, the lines of the allowed $\boldsymbol{k}$ vectors never cross the K point. The minimum (maxi-

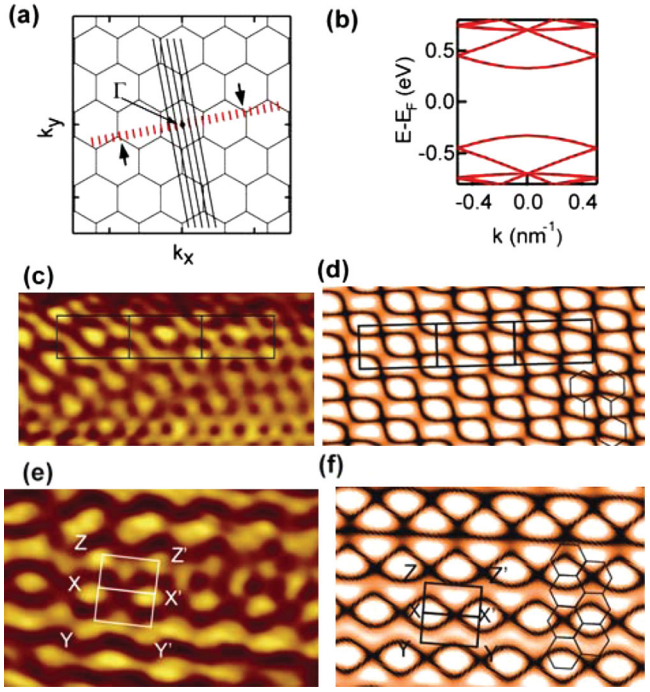

FIG. 2 (color). (a) Brillouin zones of graphene and allowed $\boldsymbol{k}$ points for the $(4, 2)$ CNT shown by long black lines. The short red lines indicate their alternative expression. The k points that give the energy minimum (maximum) in the conduction band (valence band) are indicated by arrows, which are the closest points to K and K′. (b) Calculated band structure for a CNT of $(15, -1)$. The length along the horizontal axis corresponds to the length of the red lines in (a). (c),(d) Comparison of a STM image [Fig. 1(a)] and a simulation result for a CNT of $(28, -13)$. Superimposed rectangles are included as a guide to the eye of the equivalent site. (e),(f) Comparison for $(15, -1)$. XX', YY', and ZZ' indicate the comparison.

mum) energy in the conduction (valence) band is given at $\boldsymbol{k}_{\min}$, which is on the red lines and is closest to the K or K' point [13]. In Fig. 2(a), we show the positions of $\boldsymbol{k}_{\min}$ with arrows.

The band structure can be calculated using the standard formula, and the result for $(15, -1)$ is shown in Fig. 2(b). The length of the x axis corresponds to that of the short red lines in Fig. 2(a), and the valence band maximum and conduction band minimum is given at $\boldsymbol{k}_{\min}$.

Using the parameter of $\boldsymbol{k}_{\min}$, we executed a tight-binding calculation with superposed Bloch states to simulate the interference pattern in the STM images [12,14]. We concentrate on producing a pattern for a conduction band ($V_{\text{sample}} > 0$ in STM observation). We consider a standard Bloch state based on the graphene sheet wherein the unit cell contains two carbon atoms (A and B) [3].

$$\psi(\mathbf{k}, \mathbf{r}) = \frac{C_A(\mathbf{k})}{\sqrt{N}} \sum_{\boldsymbol{R}_A}^{N} e^{i\mathbf{k}\cdot\boldsymbol{R}_A} \varphi_A(\mathbf{r} - \boldsymbol{R}_A) \pm \frac{C_B(\mathbf{k})}{\sqrt{N}} \times \sum_{\boldsymbol{R}_B}^{N} e^{i\mathbf{k}\cdot\boldsymbol{R}_B} \varphi_B(\mathbf{r} - \boldsymbol{R}_B), \quad (1)$$

where $\boldsymbol{R}_A$ and $\boldsymbol{R}_B$ indicate the coordinates of the carbon atoms A and B, respectively. C_A and C_B are normalization coefficients. We obtained eigenvalues by calculating the overlap integrals with only the nearest-neighbor atoms. The bonding and antibonding band corresponds to $+$ and $-$, respectively. If we consider the antibonding band at the Γ point, the carbon atoms have an alternative phase that gives the negative term in Eq. (1).

The one-dimensional interference wave function can be expressed by the superposition of forward and backward waves that have equal electron energy [6]. Likewise, we can form a 2D interference wave function for elastic scattering:

$$\rho \propto |\psi(\mathbf{k}_1, \mathbf{r}) + Re^{i\eta}\psi(\mathbf{k}_2, \mathbf{r})|^2, \quad (2)$$

where η and R are the phase shift and reflectivity, respectively. We fixed η at π for the entire simulation, which is based on the result of a theoretical calculation of an electronic state at end cap [15]. However, the calculated interference pattern was not sensitive to the changes of η. The Bloch states of $\boldsymbol{k}_1$ and $\boldsymbol{k}_2$ should have the same energy for elastic scattering. This condition limits the allowed wave vector, and the combination of $\boldsymbol{k}_{\min}$ and $-\boldsymbol{k}_{\min}$ satisfies this condition. Though $\boldsymbol{k}_{\min}$ is close to K, they do not coincide. A complex interference pattern is produced depending on the relative position of $\boldsymbol{k}_{\min}$ around K. The calculated ρ is expressed by mapping the amplitude two dimensionally.

We first compare a STM image and a simulation result for a CNT whose chirality is close to an armchair. The experimental and simulation results are shown in Figs. 2(c) and 2(d), respectively; the former is part of Fig. 1(a). The scale and alignment of the tube axis is the same in both panels. To clarify the similarity between Figs. 2(c) and 2(d), three rectangles ($3\boldsymbol{a} \times \sqrt{3}\boldsymbol{a}$) are superimposed. Bright spots at the four corners and the center of the rectangle are visible in both the image and simulation. In addition, wavy lines are reproduced well [16].

$\boldsymbol{k}_{\min}$ is slightly off K, which forms a modulation with a longer periodicity. In the simulation, this can be seen as a gradual change from a wavy line to a dotlike feature in the right-hand side of the panel. This is also seen in the STM image in Fig. 1(a); the wavy lines become dotlike near the end cap.

The results for a zigzag-type CNT are shown in Figs. 2(e) and 2(f). $\boldsymbol{k}_{\min}$ is rotated $\sim 30°$ from the tube-axis direction. Characteristic wavy lines along the tube-axis direction and aligned bright spots perpendicular to the tube axis are well reproduced. XX', YY', and ZZ' are shown in both panels as a guide to the eye, with a length of $\sqrt{3}\boldsymbol{a}$ and a separation of $\boldsymbol{a}$. Good agreement between the STM image and the simulation results are seen at each point. Since a long-range modulation is expected in the image along the YXZ direction, the features along YY' and those along ZZ' in the STM images are not identical.

Next, we tried to observe variations in the interference pattern in a systematic manner; in other words, we at-

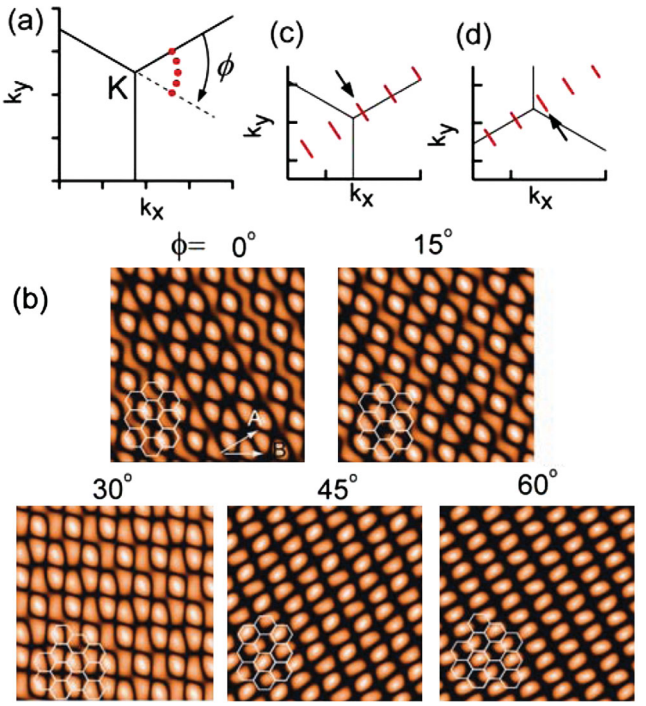

FIG. 3 (color). (a) Assumed $\boldsymbol{k}_{\min}$ positions for a simulation of the interference pattern, specified by the angle from the ΓK direction, $\phi = 0°$, $15°$, $30°$, $45°$, and $60°$ and distance from K. (b) Simulated images for each ϕ. The $\boldsymbol{k}_{\min}$ used for the simulation is set close to the direction shown by the arrow. Though there are six equivalent k points in a Brillouin zone with the same energy, the interference pattern is also aligned in this direction. (c),(d) Brillouin zones and the short lines of allowed $\boldsymbol{k}$ of the CNT of (c) $(15, -1)$ and (d) $(16, -1)$. The points closest to K and K′ are depicted by arrows.

tempted to obtain the relationship between $\boldsymbol{k}_{\min}$ and the interference pattern. $\boldsymbol{k}_{\min}$ can be expressed as a relative position from $\boldsymbol{k}$, i.e., $\Delta\boldsymbol{k} = (\boldsymbol{k}_{\min} - \boldsymbol{K})$ which can be specified by the length $|\Delta\boldsymbol{k}|$ and an angle from a symmetric line (ϕ). In Fig. 3(a), solid circles show five $\boldsymbol{k}_{\min}$ points with the same $|\Delta\boldsymbol{k}|$ and different ϕ from the direction of $\boldsymbol{\Gamma K}$. For these $\boldsymbol{k}_{\min}$ points, we calculated the interference pattern by using Eq. (2). The results for an unoccupied state are shown in Fig. 3(b).

For $\phi = 0°$, $\boldsymbol{k}_{\min}$ is located on the $\boldsymbol{MK}$ line. The Bloch states in the unoccupied state have a *positive* combination in Eq. (1). This is because they are on the line from $\boldsymbol{\Gamma}$ to $\boldsymbol{K}$, and $\boldsymbol{k}_{\min}$ is beyond $\boldsymbol{K}$. Thus, the unoccupied wave function is positioned on the band that has a bonding character at $\boldsymbol{\Gamma}$. The sign of Eq. (1) is positive, and consequently, wavy lines are clearly observed. The periodicity along arrow A in Fig. 3(b) ($\boldsymbol{\Gamma K}$ direction) is deviated from $3\boldsymbol{a}$, but the peirodicity along arrow B ($\boldsymbol{\Gamma M}$ direction) is fixed at $\sqrt{3}\boldsymbol{a}$.

For $\phi = 60°$, $\boldsymbol{k}_{\min}$ is on the symmetry line of $\boldsymbol{\Gamma K}$; this is similar to the $\phi = 0°$ case but $\boldsymbol{k}_{\min}$ does not reach $\boldsymbol{k}$. As the reverse case of $\phi = 0°$, the Bloch state corresponds to a negative combination in Eq. (1). With this configuration, the wavy patterns disappear and the periodic lattice is visible. The periodicity in the $\boldsymbol{\Gamma K}$ direction is shifted from $3\boldsymbol{a}$; however, modulation with a long periodicity is not visible.

The pattern of $\phi = 30°$ is a mixture of the two former cases. Wavy lines are clearly observed in some parts, but are not symmetric and show long-range modulation. This corresponds to the modulation observed in Fig. 1(a).

In the case where the chirality is close to an armchair, $\boldsymbol{k}_{\min}$ expectedly appears at $\phi \sim 30°$. This can be understood by using the Brillouin zone in Fig. 2(a). For armchair CNTs, the translational vector is close to the vertical direction in Fig. 3(a). Since $\boldsymbol{k}_{\min}$ is specified by the cross point of the translational vector and its perpendicular line through K, it is located in the horizontal direction from $\boldsymbol{K}$ and corresponds to $\phi \sim 30°$. With similar consideration, $\boldsymbol{k}_{\min}$ can be found at $\phi \sim 0°$ or $60°$ for a zigzag CNT.

It is intriguing to see that a large change in the interference pattern is caused by a small change in the chiral vector. A clear example of this can be seen for the zigzag CNT, and we show a comparison for cases of $(15, -1)$ and $(16, -1)$. The relation of short bars of allowed $\boldsymbol{k}$ and $\boldsymbol{K}$ is shown in Fig. 3(c) for the two cases. The upper panel corresponds to $(15, -1)$ and the lower one to $(16, -1)$. $\boldsymbol{k}_{\min}$ for both cases is indicated by arrows, located on the reverse sides of $\boldsymbol{K}$. By changing the position in the Brillouin zone, the upper panel corresponds to the case of $\phi = 0°$ and the lower panel to $\phi = 60°$. The expected difference in the interference patterns for $\phi = 0°$ and $\phi = 60°$ is clearly seen in Fig. 3(b); wavy lines are visible in the former case but disappear in the latter case. In chiral vector determination, the observation of interference patterns can play a complementary role to direct observations of the hexagonal network, as electron and photon diffraction techniques have contributed to structure determination of the materials.

We have focused our discussion on semiconducting CNTs. Similar discussions can be applied for metallic CNTs. However, as was pointed out by Kane and Mele [14], two branches of $E(k)$ curves exist in the band structure near E_f, which makes the interference patterns more complicated than those of semiconducting CNTs.

In summary, we have shown clear interference patterns near the end cap for semiconducting CNTs in STM images. We performed simple tight-binding calculations to simulate the interference patterns, in which Bloch states with $\boldsymbol{k}$ and $-\boldsymbol{k}$ wave vectors are superimposed. The calculated results for $\boldsymbol{k}_{\min}$, which gives the minimum energy in the conduction band, can reproduce the observed interference pattern very well. in addition, systematic pattern changes are confirmed with the variation of the position of $\boldsymbol{k}_{\min}$ around the K point, which is determined by the chiral vector of a CNT. The sensitivity of the diffracted waves for structure determination has been confirmed in x-ray diffraction and low-energy electron diffraction, and we believe similar techniques can be used for the Bloch state.

This research was partially supported by the Ministry of Education, Science, Sports and Culture, Japan, with a Grant-in-Aid for Scientific Research in Priority Areas 448, 2005.

*Corresponding author.
komeda@tagen.tohoku.ac.jp

[1] C. Joachim, J. K. Gimzewski, and A. Aviram, Nature (London) **408**, 541 (2000).
[2] S. J. Tans *et al.*, Nature (London) **386**, 474 (1997).
[3] R. Saito, G. Dresselhaus, and M. S. Dresselhaus, *Physical Properties of Carbon Nanotubes* (Imperial College Press, London, 1998).
[4] S. G. Lemay *et al.*, Nature (London) **412**, 617 (2001).
[5] L. C. Venema *et al.*, Science **283**, 52 (1999).
[6] M. Ouyang, J. L. Huang, and C. M. Lieber, Phys. Rev. Lett. **88**, 066804 (2002).
[7] J. Lee *et al.*, Phys. Rev. Lett. **93**, 166403 (2004).
[8] V. Meunier and P. Lambin, Phys. Rev. Lett. **81**, 5588 (1998).
[9] L. C. Venema *et al.*, Phys. Rev. B **62**, 5238 (2000).
[10] J. W. G. Wildoer *et al.*, Nature (London) **391**, 59 (1998).
[11] T. W. Odom *et al.*, Nature (London) **391**, 62 (1998).
[12] A. Rubio *et al.*, Phys. Rev. Lett. **82**, 3520 (1999).
[13] C. T. White and J. W. Mintmire, Nature (London) **394**, 29 (1998).
[14] C. L. Kane and E. J. Mele, Phys. Rev. B **59**, R12 759 (1999).
[15] T. Yaguchi and T. Ando, J. Phys. Soc. Jpn. **70**, 1327 (2001).
[16] In the simulation, we have three equivalent patterns with the same energy, which cannot be distinguished in Bloch state approximation.